Journal of South American Earth Sciences xxx (2017) 1–11

Contents lists available at ScienceDirect

Journal of South American Earth Sciences

journal homepage: www.elsevier.com/locate/jsames

Thermo-mechanical analysis of the Andean lithosphere over the Chilean-Pampean flat-slab region

Marcos A. Sánchez [a,*], Juan P. Ariza [a], Héctor P.A. García [a], Guido M. Gianni [a], M. Cecilia Weidmann [a], Andrés Folguera [b], Federico Lince Klinger [a], Myriam P. Martinez [a]

[a] CONICET, Instituto Geofísico y Sismológico Ing. Volponi, Universidad Nacional de San Juan, Ruta 12, Km. 17, CP 5407, San Juan, Argentina
[b] CONICET, Inst. Estudios Andinos "Don Pablo Groeber", Dep. Cs. Geol, FCEN, U.B.A, Buenos Aires, Argentina

ARTICLE INFO

Article history:
Received 1 July 2017
Received in revised form
25 September 2017
Accepted 30 September 2017
Available online xxx

Keywords:
Heat flow
Curie Point Depth
Chilean-Pampean flat-slab
Magnetic data
Elastic thickness

ABSTRACT

Flat subduction segments are generally related to cold lithospheric zones, which suggest low Heat flow values and therefore a deeper Curie isotherm. In this study we perform a geophysical analysis by using high - resolution magnetic data, obtaining shallower Curie point depths through the Chilean-Pampean flat-slab zone. Then using temperatures from borehole data and Curie Point Depths, we performed a Heat Flow map which indicates the existence of mean to high thermal anomalies across the Chilean - Pampean flat-slab. These results were contrasted with Elastic Thickness map (Te) obtained from the Eigen-6C4 gravity model. Low Te values acquired indicate zones with weak mechanical behavior in correspondence to thermal anomalous zones. This spatial correlation suggests that the local high thermal anomalies are conditioning the mechanical behavior of the lithosphere in the study area and the locations of geothermal sources. Overall, our results indicate that the thermal structure of the flat-slab segment is more heterogeneous than previously thought. This has implications for evolution, maturity and fluid circulation in foreland basins of the Main and Frontal cordilleras and the Precordillera thrust belts. Finally, further studies will allow improving our database as well as extending our understanding of the thermal structure of the Chilean-Pampean flat-slab.

1. Introduction

Variations in subduction styles, and in particular from steep to flat subduction angles, have a major impact on the thermal and rheological structure of the upper plate (Gutscher, 2002). When compared to steep subduction angles, flat subduction segments are generally related to lower heat flow ($20-70\ mW/m^2$ vs $50-120\ mW/m^2$) (e.g., Henry and Pollack, 1988; Currie et al., 2002; Manea et al., 2005, 2016; Marot et al., 2014), as it is well illustrated in heat flow analyses from flat-slab areas in Mexico ($13–22\ mW/m^2$, Ziagos et al., 1985), Peru ($\sim 20-70\ mW/m^2$) (Henry and Pollack, 1988) and Central Chile ($\sim 40-45\ mW/m^2$, Collo et al., 2017). Moreover, low heat flow in flat-slab subduction zones can be easily observed from global heat flow maps indirectly derived from seismic models based on surface waves and Curie depth analyses (e.g., Shapiro and Ritzwoller, 2004; Li et al., 2017). The sub-lithospheric cooling effect in these settings is mainly due to the within-plate expelling of the mantle wedge during flat slab development, which diminishes drastically the asthenospheric contribution to heat flow (Gutscher et al., 2000; Manea and Manea, 2011). On the contrary, steeper subduction zones are characterized by the presence of a broad asthenosphere wedge and the local effect of volcanism that together produce higher heat flow at distances between ~300 and 400 km away from the trench (e.g., Henry and Pollack, 1988).

The area of interest in this contribution is the sub-horizontal subduction zone between $\sim 28°$ and $\sim 33°$ S, known as the Chilean - Pampean flat slab zone, characterized by the absence of volcanism in the last 4-2 My, the increase of intraplate seismicity related to neighboring segments (Barazangi and Isacks, 1976; Jordan et al., 1983; Alvarado et al., 2009; Gans et al., 2011), the widespread basement foreland deformation (Ramos et al., 2002) and dynamic subsidence at the leading edge of the flat segment (Dávila and Lithgow-Bertelloni, 2015). Regional heat flow analysis from Hamza et al. (2008) determined values ranging from $80\ mW/m^2$ to $60\ mW/m^2$ over the Chilean-Pampean flat-slab zone.

* Corresponding author.
E-mail address: 1marcossanchez@gmail.com (M.A. Sánchez).

https://doi.org/10.1016/j.jsames.2017.09.036
0895-9811/

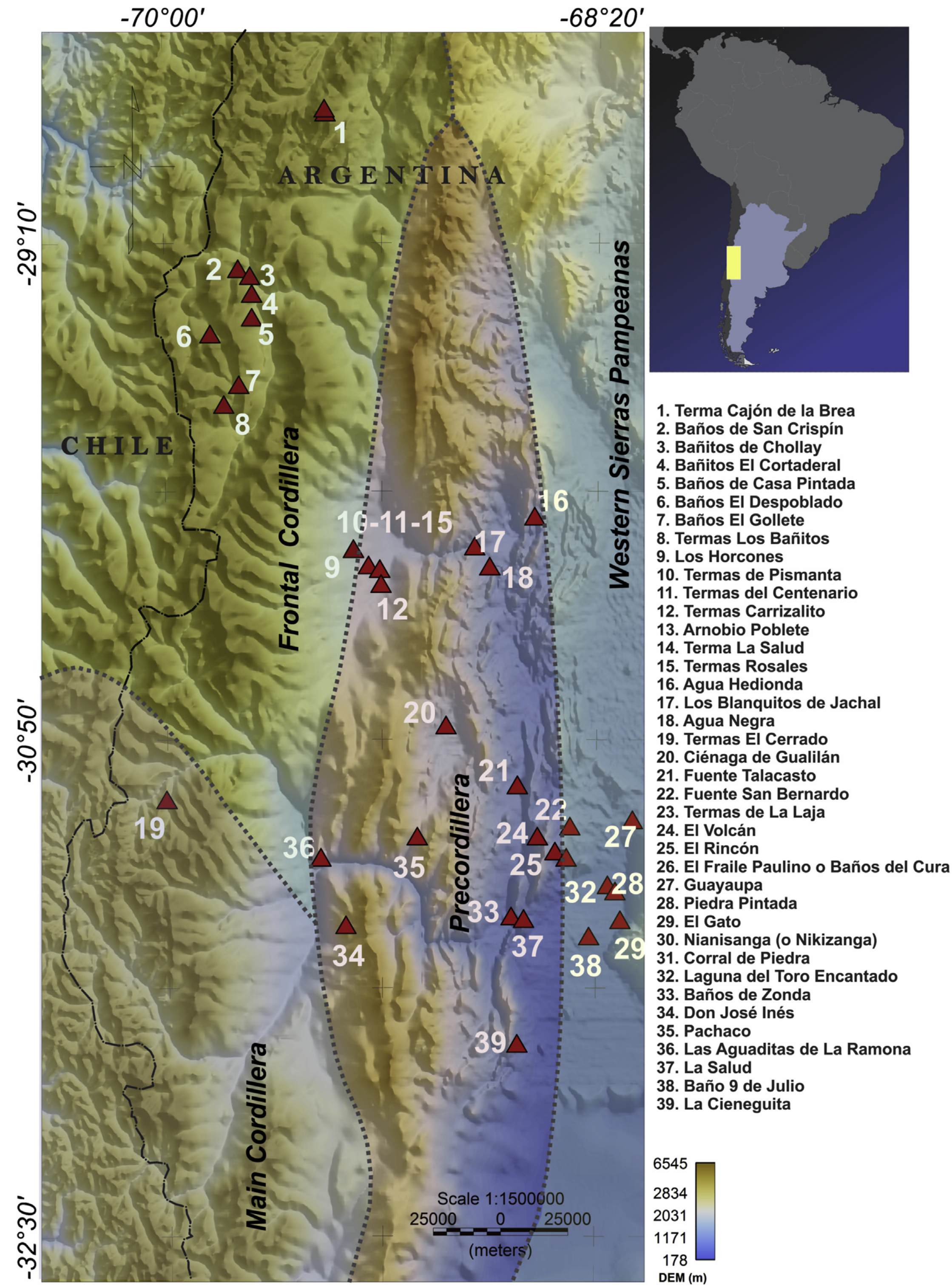

Fig. 1. Location of the area of interest in the Chilean-Pampean flat-subduction zone. Red triangles show the distribution of thermal manifestations (Pesce and Miranda, 2003) over a digital elevation model ETOPO1 (Amante and Eakins, 2009) whose relation to heat flow is one of the objectives of this work. (For interpretation of the references to colour in this figure legend, the reader is referred to the web version of this article.)

Ruiz and Introcaso (2004), with a different approach, carried out a local heat flow analysis based on a Curie depths point determination from field magnetic data over the Precordillera and Western Sierras Pampeanas (Fig. 1) obtaining comparable values in the range between $43 - 80\ mW/m^2$. Collo et al. (2011) explored clay mineral indexes in synorogenic sequences in the northern sector of Western Sierras Pampeanas (Fig. 1) to determine basin maturity and geothermal gradient during diagenesis. These authors obtained average heat flow values between $33\ mW/m^2$ and $42\ mW/m^2$ consistent with the absence of an asthenospheric wedge controlled

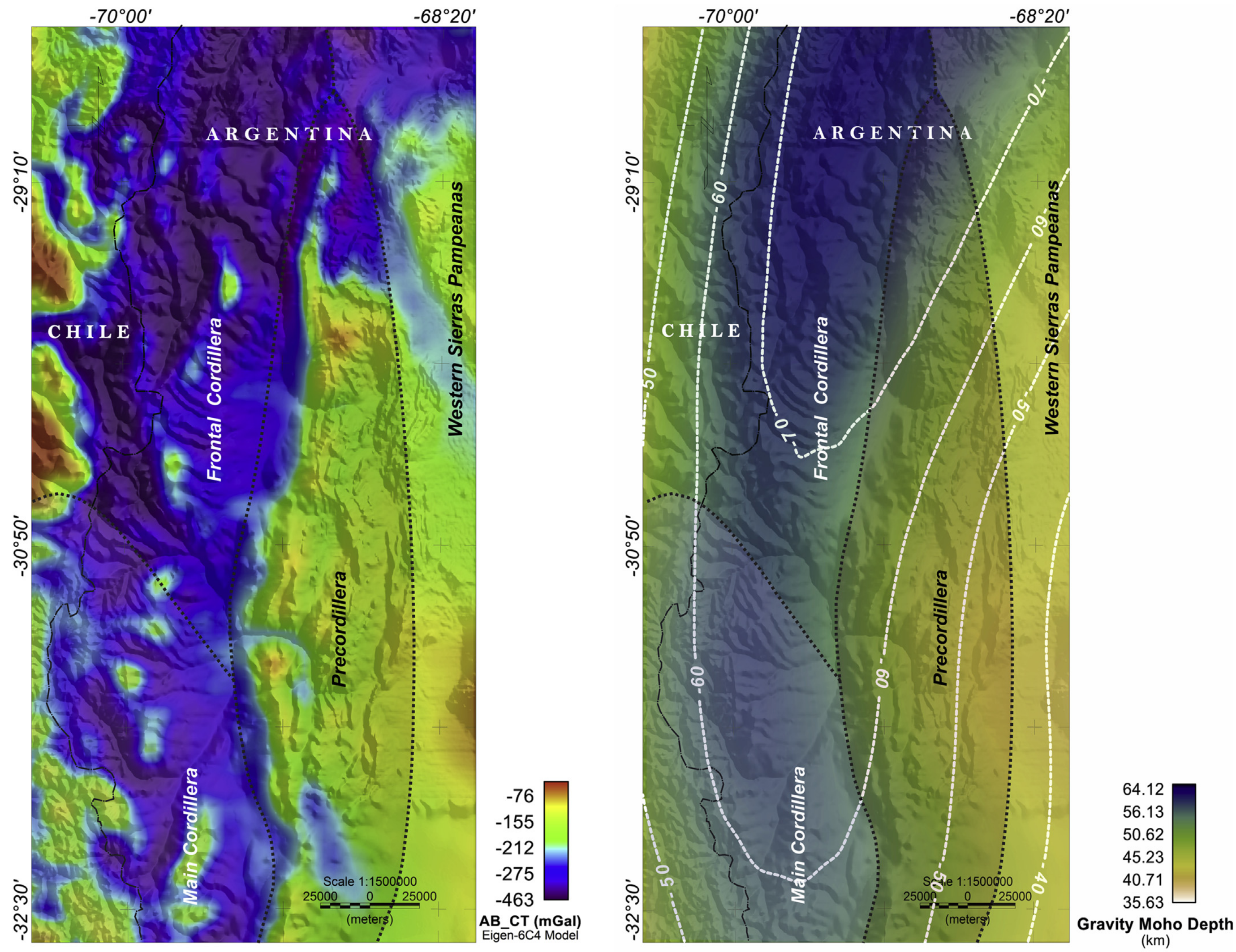

Fig. 2. a) Terrestrial and aerial magnetic databases distribution used for computing the magnetic anomaly. b) Magnetic Anomaly obtained by aerial databases obtained from Argentinean Mining Geological Service, (SEGEMAR). The magnetic anomalies values were calculated on a regular grid cell size of 1 × 1 km, using the Minimum Curvature method (Briggs, 1974).

by the geometry of Chilean-Pampean flat-slab. The later interpretation was supported by Weidmann et al. (2017) based on a Curie Point Depths analysis that comprised the northern sector of Western Sierras Pampeanas. More recently, Collo et al. (2017) used a compilation of temperature data from oil wells within the Chilean-Pampean flat-slab segment to construct a regional a heat flow (q) map, obtaining results ranging between $20-70$ (mW/m^2). In addition, these authors carried out a Curie Point Depth analysis from aeromagnetic data and found values of $26-45$ (km) to the east of the region analyzed in this work by using the same methodology, but with less CPD than that calculated in this contribution.

In this contribution we analyzed deep magnetic anomalies from aeromagnetic data. Then, we define a lithospheric model based on the inversion of magnetic susceptibilities to obtain the depth of the Curie Isotherm. We present a heat flow map of the study area derived from higher resolution data from our Curie Point Depth analysis and borehole data. In order to analyze a potential relation between the thermal regime and the mechanical behavior of the lithosphere in the study area, we carried out an estimation effective elastic thickness (Te), a proxy of long-term lithospheric strength (Watts, 2001).

Finally, our results show that the thermal structure of Chilean-Pampean flat-slab zone is more complex than previously thought, which has implications for foreland basin analysis in the Main Cordillera, Frontal and Precordillera and related geothermal resources in the those regions.

2. Tectonic setting

The Chilean-Pampean flat-slab is one of the ten active flat subduction settings on the Earth and is linked to the subduction of the oceanic Nazca plate beneath South America (Barazangi and Isacks, 1976, 1979; Cahill and Isacks, 1992; Gutscher et al., 2000). Most recent studies propose that the change from shallow to flat subduction began at ~19 Ma (Jones et al., 2014, 2015, 2016), achieving a completely flat geometry at around ~7-6 Ma (Ramos et al., 2002; Gans et al., 2011; Gutscher et al., 2000; Kay et al., 1991; Kay and Mpodozis, 2002). This process has been linked to the registered eastward expansion of the Neogene magmatism and subsequent arc gap between 27 and 33°S, and the development of a broken foreland zone in latest Miocene to Pliocene-Quaternary times (Allmendinger et al., 1990; Cahill and Isacks, 1992; Jordan et al.,

Please cite this article in press as: Sánchez, M.A., et al., Thermo-mechanical analysis of the Andean lithosphere over the Chilean-Pampean flat-slab region, Journal of South American Earth Sciences (2017), https://doi.org/10.1016/j.jsames.2017.09.036

1983; Kay et al., 1988, 1991; Kay and Abbruzzi, 1996; Pilger, 1981; Smalley and Isacks, 1987; Stauder, 1973). The geometry of the Chilean-Pampean flat-slab has been defined mainly from seismic and geophysical analysis (Barazangi and Isacks, 1976; Tassara et al., 2006; Alvarado et al., 2007; Anderson et al., 2007; Gilbert et al., 2006; Gimenez et al., 2009; Gans et al., 2011; Marot et al., 2014). At these latitudes the Nazca plate lays sub-horizontally for ~400 km, from the trench, before plunging into the mantle with "normal" angularity (~30–45° to the East).

There are different recent proposals for the generation of the flat-slab subduction. These mechanisms include: (a) the subduction of buoyancy anomalies such as aseismic ridges (Cloos, 1993; Gutscher et al., 1999); (b) the fast overriding of a continent over young oceanic lithosphere (Van Hunen et al., 2002); (c) the hydrodynamic suction force due to thick continental roots that couples the subducting slab with the overriding plate (Manea et al., 2012); (d) mantle plume-subduction zone interaction, where the slab is dynamically uplifted as the buoyant plume is subducted (Murphy et al., 1998; Gianni et al., 2017). However, the actual mechanism that produces the Chilean-Pampean flat-subduction is still controversial.

2.1. Magnetic database

The magnetic database used in the present contribution comes from: i) A terrestrial dataset which was only used as a control tool to unify aerial databases, and ii) three aerial databases available in a total magnetic field grid, obtained from Argentinean Mining Geological Service (SEGEMAR). These datasets were corrected by the daily variation of blocks 4, 9 and 17. Such reductions were made by the companies of acquisition (Dobrin, 1976). Block 4 corresponds to the northern Precordillera area between San Juan and La Rioja provinces, where the nominal flight height was 140 m. Block 9 corresponds to Frontal Cordillera in San Juan Province, and was measured to a nominal flight height of 120 m. The last database used is Block 17 corresponding to southern Precordillera between San Juan and Mendoza provinces, with a nominal flight of 120 m.

The magnetic anomaly was calculated for each block, by removing the International Geomagnetic Reference Field (IGRF), from each block at the acquisition date (Blakely, 1995). Then, we built an anomaly map (See Fig. 2), by using all databases following the methodology proposed by Cheesman et al. (1998) and Ruiz et al. (2011). A high resolution grid was calculated with cell size of 250 m × 250 m, using the Minimum Curvature method (Briggs, 1974).

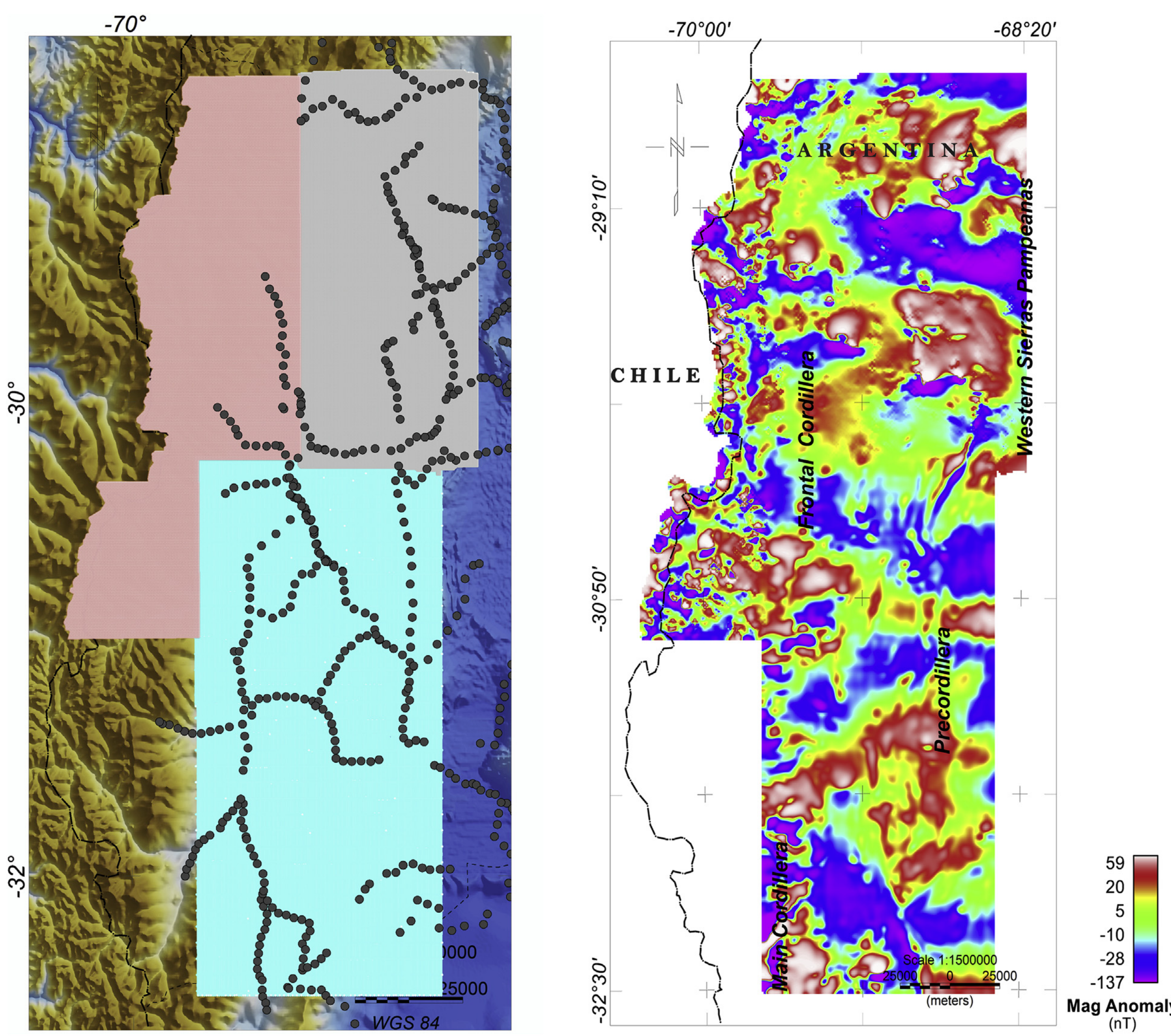

Fig. 3. Curie Isotherm Depth obtained, from the Program CuDePy (Soler, 2015).

Table 1
Summary of *q* values obtained from Oil-wells and magnetotelluric measures over the study area (Collo et al., 2017).

Source	q (mW/m^2)
Matagusanos Well (MA)	46
Las Toscas Well (LTs)	58–68
Arbol Blanco (WellSE.AB.X-1)	63
Sierra de las Peñas (SP)	56
Pozuelos Well (PO)	45
Borzotta et al. (2009)	36–40
Hamza et al. (2005) – Cordillera	103 ± 78
Hamza et al. (2005) – Precordillera	54 ± 25

3. Curie Point Depth estimation

The origin of terrestrial magnetism is basically the earth outer core and the crust. The mantle is not considered a generator of the geomagnetic field due the demagnetization of ferromagnetic minerals around 600 °C (Curie temperature - Hinze et al., 2013; Blakely, 1995). The paramagnetic materials are those that, when exposed to a Magnetic field, generate a magnetization in the same direction of the field, however, when the field stops acting, their magnetization returns to zero. On the other hand, the ferromagnetic materials are those that behave in a similar way to

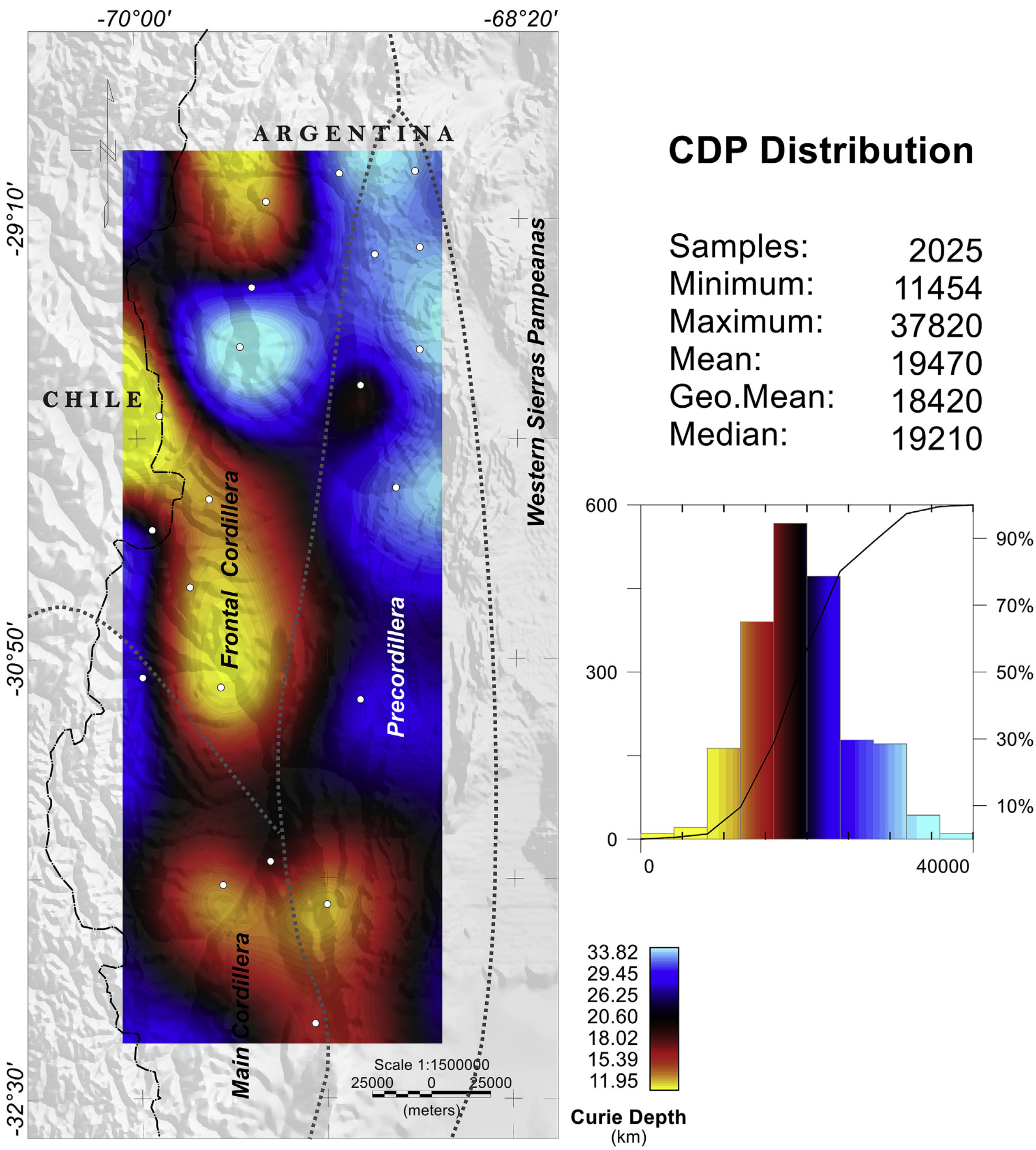

Fig. 4. Heat Flow Map obtained by Curie Point Depth.

paramagnets in the presence of an external field. However, when the external magnetic field stops acting, the material yields a non-zero remaining magnetization. Reaching this threshold or above it (Curie temperature), materials undergo a phase transition and become paramagnetic materials, meaning that they no longer have remnant magnetization.

The average global geothermal gradient is about 25 $^\circ C/km$ near the earth surface (Alfe et al., 2003; Vlaar et al., 1994). This gradient indicates that within the earth crust the Curie temperature of ferromagnetic rocks is exceeded. The depth where this process takes place is known as Curie Point Depth, or Curie Depth. Below that depth, it is considered that there are no sources of magnetic field within the lithosphere. This means that if we know the petrophysical properties of the rocks present in the crust we can estimate the Depth of the Curie Isotherm (Ross et al., 2006). However, this implies a first approximation because the demagnetizing temperatures (Curie temperature) can vary up to hundreds of degrees depending on rock composition.

In this respect, Frost and Shive (1986) demonstrated that the lower part of the crust is magnetite-rich, being the only significant magnetic source. The temperature of the magnetite curve is increased with the pressure of 1.8 $^\circ C/kbar$. From this, these authors suggest that deeper rocks lose magnetization at about 600 $^\circ$ C.

The conventional techniques to estimate the depths of magnetic sources are based on statistical analysis of the anomaly in frequency domain by using the power spectrum. To simplify the calculation, we assume the magnetized crust as a horizontal semi - infinite plate whose top and bottom are found at depths of Zt, and Zb, respectively. If its magnetization is uniformly random and not correlated, then the Power Spectrum of the magnetic anomalies can be related to its characteristic depths through the following equation (Blakely, 1995),

$$ln\Phi'_{\Delta T}(\mathrm{k}) = lnA - 2\mathrm{Z_t}k + 2ln \tag{1}$$

where $\Phi'_{\Delta T}$ is the averaged Power Spectrum of the magnetic anomaly, k is the module of the wave vector and A is a constant with no physical significance.

The above assumption over a magnetized slab is valid because it contains all the ferromagnetic crust materials, and no magnetized bodies can be found below it. So, the Curie Depth Point can be linked to the bottom of this magnetized slab, *Zb*.

With the aim to calculate the Curie isotherm depth in the study area, we have applied a method developed by Soler (2015) derived from the ones proposed by Ross et al. (2006) and Ravat et al. (2007).

The method developed by Soler (2015) uses of the Levenberg–Marquardt least square fitting algorithm for non-linear problems in order to adjust the last equation on the previously radially averaged power spectrum of the magnetic anomalies. This allowed us to estimate several Curie point depths through an interactive selection of square sub-regions ($10x10\,Km$) of the magnetic anomaly grid. Then, by using the aerial and land magnetic database explained above, we obtain several estimates of the Curie depth. These specific values were then regularized to obtain an aerial distribution as shown in Fig. 3.

4. Heat flow determination

The equation which combines the heat flow (q), the Curie Temperature (θc), and the Curie Depth point (Dc) in a region where there are not any sources or sinks of heat between the Earth surface and the Curie point depth (Tanaka et al., 1999; Ruiz and Introcaso, 2004), is:

$$q = k\ \theta c/Dc \tag{2}$$

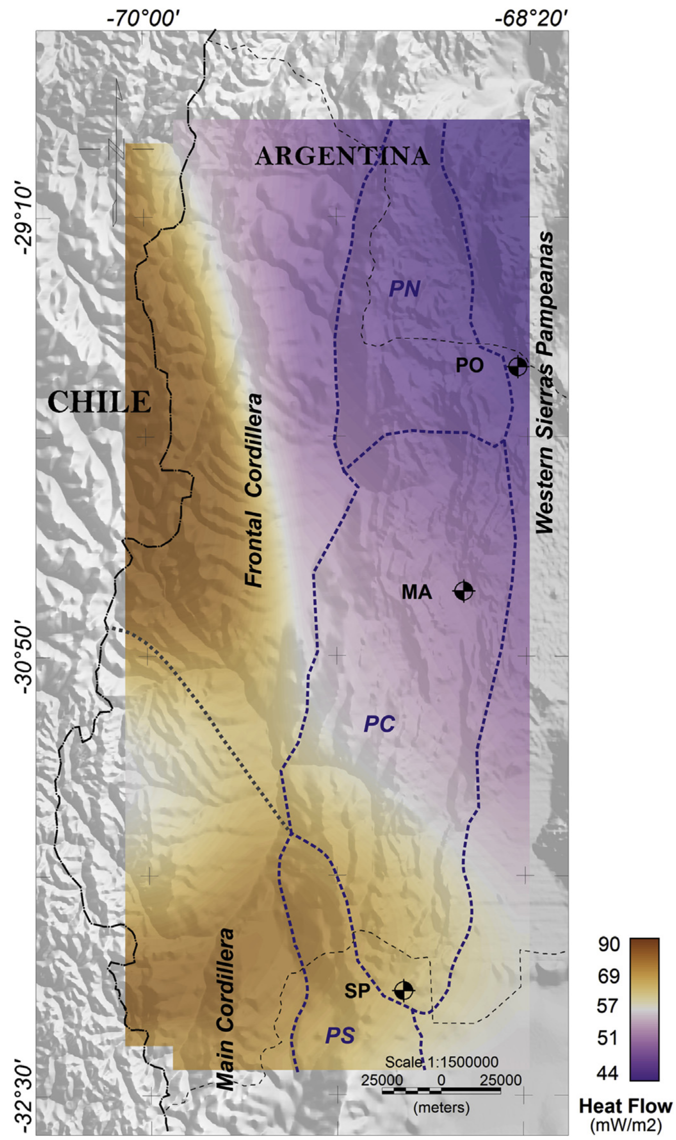

Fig. 5. a) Bouguer anomaly map obtained from the EIGEN-6C4 model (http://icgem.gfz-potsdam.de/ICGEM/ICGEM.html), which combines marine, terrestrial and satellite data (Förste et al., 2014). Corrected by topography. b) Inverted Gravity Moho Depth. White dashed lines show contour lines of Moho depth obtained by Gemma Global Model (Sampietro et al., 2013; Reguzzoni and Sampietro, 2015).

This implies that we can make indirect calculations of the crustal heat flow from a good coverage of magnetic data, as in our case, and then by applying an appropriate statistical approach we can determine the heat flow value from the Curie depth point. The value of q calculated is mainly related to the heat conduction from the temperature at the Lower Crust.

For the study area the average geothermal gradient recently obtained by Collo et al. (2017) is $dT/dz = 31^\circ C/km$. From Fig. 3, the calculated average Curie Isotherm depth for this zone is $Dc \sim 20\ km$, and so, from Eq. (2), $\theta c = 620^\circ C$ or $893^\circ K$.

Over the Central Andes, Springer and Förster (1998), Ruiz and Introcaso (2004) and others have used different values for the coefficient of thermal conductivity (k). We assumed $k \sim 2.5\ W^{-1}\ m^{-1}\ ^\circ K^{-1}$ for calculus due to the existence of volcanic rocks and sediments which have a different thermal behavior in correspondence with Li et al. (2017) who proposed this value for k in continental zones using to the Earth Magnetic Anomaly Grid of

Please cite this article in press as: Sánchez, M.A., et al., Thermo-mechanical analysis of the Andean lithosphere over the Chilean-Pampean flat-slab region, Journal of South American Earth Sciences (2017), https://doi.org/10.1016/j.jsames.2017.09.036

2-arc-minute resolution (Maus et al., 2009; EMAG2, http://geomag.org).

A wide range of values of heat flow on this area has been proposed recently. Table 1 summarizes the different surface heat flow (SHF) values found. Considering all of these, we have used a mean q value of $\sim 70\ mW/m^2$.

In a first step, SHF values from boreholes within the area have been used as a constraint. Then, by assuming a mean regional Curie point depth $Dc = 20\ km$ (see histogram on Fig. 3) and a mean heat flow $qm \sim 70\ mW/m^2$, we have obtained $k\ \theta c \cong 1400\ Wm^{-1}$ from Eq. (2).

In Fig. 4 a heat flow map calculated from Curie Point Depth, considering $qc = 1400\ Wm^{-1}$, shows some correlation with the heat flow map published by Ruiz and Introcaso (2004). Mismatches between them are most likely related to the resolution of data used for CDP calculus and recent estimation of parameters of gradient and k for the study region.

5. Gravity database

Satellite and high-resolution gravity field models based on a combination of satellite and terrestrial data are available in spherical harmonic expansion (e.g. EGM2008, Pavlis et al., 2008). Pure satellite models present lower resolution than combined models, although they are accurate for interpretation of large-scale structures, especially in high and inaccessible regions such as certain zones of the high Andes where terrestrial data are sparse due to the limited access (Álvarez et al., 2012, 2014, 2015; Braitenberg et al., 2011; Köther et al., 2012).

Earth Gravity Field models are presented as sets of coefficients of a spherical harmonic approximation of the gravity field up to a maximum degree ($N\ max$), which controls the spatial resolution of the model (λ) (Barthelmes, 2009; Hofmann-Wellenhof and Moritz, 2006; Li, 2001). Köther et al. (2012) explained that combined gravity models can be used to study relatively smaller geological features, while satellite models alone are not appropriate for this scale due to their lower spatial resolution.

In order to calculate different quantities related to a longer wavelength characteristic of the gravity field (Gravity Moho and Elastic Thickness), the Bouguer anomaly data used was obtained from EIGEN-6C4 model (http://icgem.gfz-potsdam.de/ICGEM/ICGEM.html; Barthelmes, 2014), which combines terrestrial, marine and satellite data GOCE, GRACE and LAGEOS. They are available in a grid of 181 × 241 nodes which are equispaced every 0.05° (Förste et al., 2014).

In this work, a typical topographic correction is applied to the gravity data that combines the algorithms developed by Kane (1962) and Nagy (1966). The objective of this is to correct the excesses and mass defects contemplated by the slab of Bouguer (see Fig. 5). The obtained anomaly map emphasizes the strong effect of the Andean root reaching values > 468 $mgal$. Short-wavelength anomalies that correspond to bodies located in the upper crust are also noted.

From this gravity database we performed an inversion to obtain the Moho depth. The values used on this are shown on Table 1.

Table 2
P waves velocity and densities considered in this work. (See more details in manuscript).

	P waves velocities (***km/s***)	Density (***g/cm***^{3})
Topography	6.32	2.67
Upper Crust		2.70
Lower Crust		2.90
Upper Mantle	7.97	3.30

Then, we have used the global GEMMA model ($n = 2190$) to compare the gravity Moho model calculated by inversion (Sampietro et al., 2013; Reguzzoni and Sampietro, 2015). Although the results show some quantitative differences, mainly due to the fact that GEMMA uses a global density, isobaths show a similar morphology than the calculated Moho.

5.1. Estimation of elastic thickness

In order to examine the relation between the thermal regime revealed from the above described analyses and the strength of the lithosphere over the Chilean-Pampean flat slab, we did a local high-resolution analysis of the lithosphere rigidity (D). This parameter is related to the thermal state, composition and rheological properties of the crust as well as to the flexural rigidity (Lowry et al., 2000; Introcaso, 2006). Frequently, this value is expressed through the elastic thickness of the lithosphere (Te). Watts (2001) explained that long term geological loads could give an elastic behavior to the lithosphere by flexure. Usually, when the load is located far away from the margin plate, the lithosphere is represented by an infinite two-dimensional elastic plate model overlying the relatively fluid substrate (mantle). On the other hand, when the load is near the plate margin, such as in coastal areas, the model used corresponds to a broken plate or semi-infinite plate (Watts, 2001; Turcotte and Schubert, 2002). In this contribution we have considered the first approach, since the study area is located relatively far from the margin (~250 km). The flexural rigidity of the plate could be defined by making assumptions regarding the Young modulus ($E = 100GPA = 10^{11}N/m^2$) and the Poisson ratio ($\nu = 0.25$), and the Elastic thickness (Te), with the following equation:

$$D = \frac{ET_e^3}{12(1-\nu^2)} \tag{3}$$

The effective elastic thickness was calculated by using a Python code of Soler (2015) and from spectral methods developed by Garcia et al. (2015). These considered that the load is distributed into a whole plane xy, where the deflection will be given by $w(x,y)$ and the rigidity for a big region is variable $D(x,y)$. In this work we considered horizontal stress equals zero. The code requires two data inputs: the ETOPO1 topography (Amante and Eakins, 2009), and the gravity Bouguer anomaly (Fig. 5a) including the topographic correction of this (AB_{ct}). The calculus consists in a determination of the gravimetric deflection from the ABCt for the whole study area. For this, a density contrast between the upper mantle and lower-crust ($\rho_m - \rho_{lc}$) was used inside the Parker-Oldenburg algorithm (Parker, 1973; Oldenburg, 1974). The code contains an interface that allows choosing windows with variable positions and sizes, being Te constant inside each one. Additionally, we have used windows with sizes of 70 x 70 km.

Several values of Te are considered for a window, and then their deflection is calculated (w_{loc}). For each chosen value we considered the topographic load of the whole study area in both horizontal directions. The obtained w_{loc} values are compared with the gravity deflection inverted w_{inv} inside the chosen window. The actual Te is that which presents the minimum rms (root mean square). The densities used are shown on Table 2. These were obtained from velocities of P waves found by Chulick et al. (2013). Each one was converted by using the equation of Brocher (2005). All found values are consistent with previous contributions (Cornaglia et al., 2009; Lince Klinger et al., 2011; Weidmann et al., 2013; Álvarez et al., 2015; Sánchez et al., 2017). For the density of topography (ρ_t) we used a value of 2.67 g/cm^3 following Hinze (2003). Finally, a grid of elastic thickness values was made by using the 433 calculated estimations (Fig. 6).

Please cite this article in press as: Sánchez, M.A., et al., Thermo-mechanical analysis of the Andean lithosphere over the Chilean-Pampean flat-slab region, Journal of South American Earth Sciences (2017), https://doi.org/10.1016/j.jsames.2017.09.036

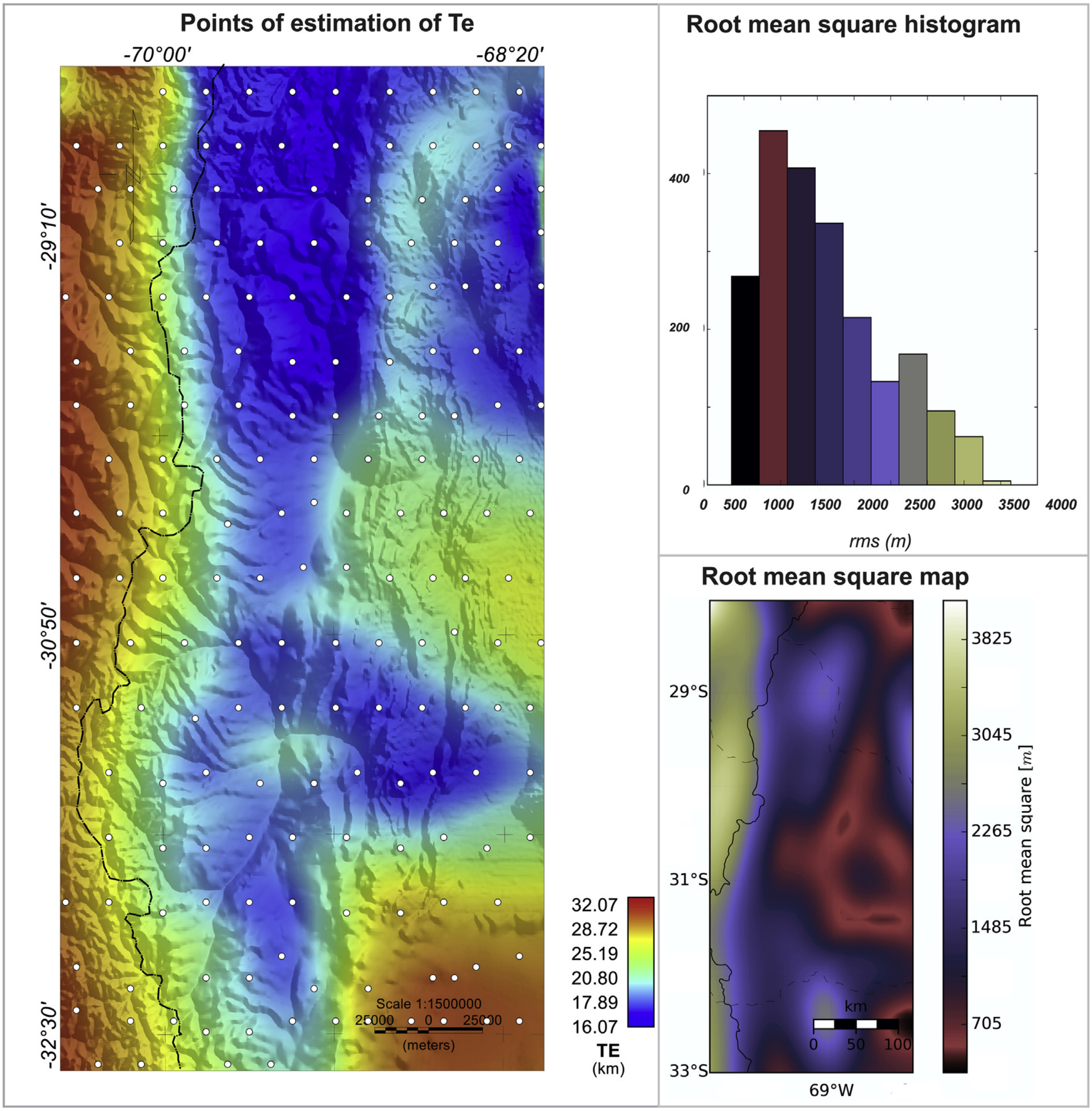

Fig. 6. Elastic Lithospheric Thickness obtained by inversion of gravity deflection. White points indicate location where Te was calculated through Soler's Python Code (Soler, 2015) by rms values comparison between inverted and flexural Moho. The results are shown on a map and on a histogram that indicates the convergence of solutions (Garcia et al., 2015).

6. Results and discussion

The spectral analysis of the aerial magnetic database allowed us achieving a Curie depth point map at a higher resolution than any other previous calculation of this isotherm over the Chilean-Pampean flat-slab zone (Ruiz and Introcaso, 2004; Collo et al., 2017). Thus, the analysis of the Curie depth map presented on Fig. 3 shows a wide range of depths with anomalous shallow values between $\sim 12 - 15$ km arranged in a NNW-SSE trending fringe over the Main and Frontal cordilleras and the southern sector of the Precordillera. On the eastern sector of the study area, the isotherm becomes deeper achieving values between $\sim 20 - 30$ km over the Central and northern sector of Precordillera, Western Sierras Pampeanas and the northernmost extreme of the Frontal Cordillera. This is consistent with the results obtained in recent works of Weidmann et al. (2017) and Collo et al. (2017) over the Western Sierras Pampeanas. Our heat flow map (q) (Fig. 4) obtained by inversion using new parameters of thermal conductivity (k) (Li et al., 2017) and oil-wells gradient registers, indicates values ranging between $55 - 95\ mW/m^2$.

Remarkably, an anomalous zone with high values between $85 - 95\ mW/m^2$ is coincidental with the shallow Curie depth area described above. Taking into account that at a global scale, areas with heat flow $> \sim 70\ mW/m^2$ and $< \sim 40\ mW/m^2$ are considered above and below normal (Blackwell, 1969, 1971; Roy et al., 1972), our results suggest a rather normal to high heat flow regime in the study area (Fig. 5). These results contrast with heat flow estimates from similar analyses of regional character ($43 - 60\ mW/m^2$, Ruiz and Introcaso, 2004; $20 - 70\ mW/m^2$, Collo et al., 2017) (Figs. 6 and 7). Estimation of elastic thickness

Please cite this article in press as: Sánchez, M.A., et al., Thermo-mechanical analysis of the Andean lithosphere over the Chilean-Pampean flat-slab region, Journal of South American Earth Sciences (2017), https://doi.org/10.1016/j.jsames.2017.09.036

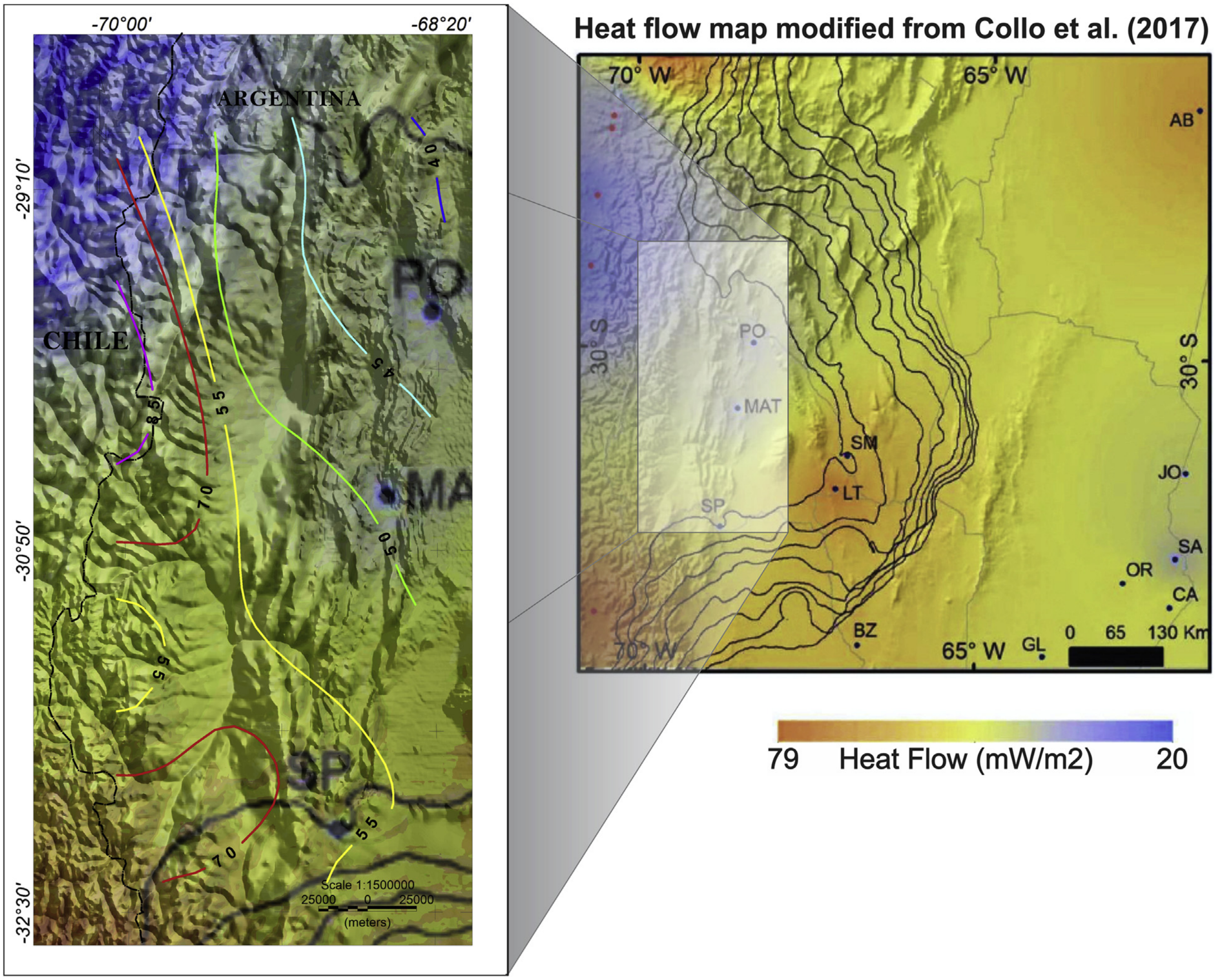

Fig. 7. Heat flow isolines obtained in present contribution (in colors), in contrast with the previous Heat Flow map presented by Collo et al. (2017). (For interpretation of the references to colour in this figure legend, the reader is referred to the web version of this article.)

derived from the analysis of high-resolution EIGEN-6C4 gravity model shows a striking correlation with the described heat flow and Curie depth results. In this sense, a zone of low elastic thicknesses with values between 16 and 32 km, spatially correlates with the area where a high heat flow and shallower Curie isotherm was determined (Figs. 3, 4 and 6). The observed spatial correlation with the analyzed parameters could indicate that the local high thermal anomaly is conditioning the mechanical behavior of the lithosphere in the study area. It is remarkable that the locations of geothermal sources shown in Fig. 1 are consistent with the high heat flow and low elastic thickness values found. Collectively, our results suggest that the thermal structure of the Chilean-Pampean flat-slab is more heterogeneous than previously thought.

Variations in the surface heat flux can be differentiated in wavelengths. While short wavelengths might be associated with structuration and/or variations in the composition and thicknesses within the crust, longer wavelengths have been interpreted as terranes accreted to the Gondwana margin with different ages or variations in heat flux to the base of the lithosphere. Since the region studied in this manuscript encompasses the south-western portion of the flat subduction region, heat flow variations are likely associated with smaller wavelengths than those that could be generated by variations in the subduction regime. In this sense, Collo et al. (2017) interpreted the anomaly in the intermontane valleys between the Mascasín and Beazley wells (BHF 57 and 68 $mW/m2$ and shallow CPD) as associated with the evolution of the basement-involved Sierra de Valle Fértil megathrust, although more studies are needed to arrive to a suitable explanation. Similarly, higher short-wavelength anomalies determined on this study over the Frontal Cordillera could be related to deep basement structures that characterize this morphostructural unit (Fig. 4). Nevertheless, in the Precordillera region the correlation between deformation style and heat flow is not straightforward (Fig. 4). While a relatively higher heat flow anomaly is described in the thick-skinned southern Precordillera (Cortés et al., 2006; Cortés et al., 2014), thin-skinned deformation in the central region of Precordillera and thick-skinned style of deformation in the Eastern as well as the Northern Precordillera, correlate with relatively lower heat flow anomaly values (Fig. 4). Hence, the source of the thermo-mechanical structure of the study area is not clear and other studies with similar approaches of regional character — perhaps the double inversion of potential methods and seismology data— will be necessary in order to determine its origin. Noteworthy, similar high heat flow anomalies have been previously found over the Mexican flat-slab (Manea and Manea, 2011). Considering that heat flow affects the evolution, maturity and fluids within sedimentary basins, if our data is representative of the past thermal regime, foreland basins linked to the Frontal Cordillera and the Precordillera may have followed a different thermal evolution compared with "refrigerated" basins in the broken foreland area. This expression was defined by Collo et al. (2017) to describe low geothermal gradients determined in inter-montane basins over the flat-slab region. In this sense, there are various surface evidence of geothermal manifestations in different sectors in the study area that are located over the low elastic thickness-high heat flow zone determined in this study (Pesce and Miranda, 2003) (Fig. 1).

7. Conclusions

Curie depth point map obtained from frequential analysis of magnetic high-resolution data and heat flow estimation derived from these data and constrained by oil-well data indicates anomalous thermal zones above the Chilean-Pampean flat-slab. High heat flow and shallow Curie isotherm are coincident with areas of low elastic thickness values derived from EIGEN 6C4 gravity model. This spatial correlation suggests that the local high thermal anomaly is conditioning the mechanical behavior of the lithosphere in the study area and the locations of geothermal sources. Overall, our results indicate that the thermal structure of the flat-slab segment is more heterogeneous than previously thought. This has implications for evolution, maturity and fluids in foreland basin of the Main and Frontal cordilleras and the Precordillera thrust belts. Finally, further studies will allow improving this database as well as extending the understanding of the thermal structure of the Chilean-Pampean flat-slab.

Acknowledgements

We would like to express our thanks to the Grosso Group Company and the Argentinean Geological Mining Service (SEGEMAR) for their aero-magnetic flight data. This study has been partially financed by projects PIO 150-201501-00039-CO (Oriented Research Projects - CONICET- Secretariat of Science and Technology. Government of San Juan).

References

Alfe, D., Gillan, M.J., Price, G.D., 2003. Thermodynamics from first principles: temperature and composition of the Earth's core. Mineral. Mag. 67 (1), 113–123.
Allmendinger, R.W., Figueroa, D., Snyder, D., Beer, J., Mpodozis, C., Isacks, B.L., 1990. Foreland shortening and crustal balancing in the Andes at 30 S latitude. Tectonics 9 (4), 789–809.
Alvarado, P., Beck, S., Zandt, G., 2007. Crustal structure of the south-central Andes Cordillera and backarc region from regional waveform modelling. Geophys. J. Int. 170 (2), 858–875.
Alvarado, P., Pardo, M., Gilbert, H., Miranda, S., Anderson, M., Saez, M., Beck, S., 2009. Flat-slab subduction and crustal models for the seismically active Sierras Pampeanas region of Argentina. Geol. Soc. Am. Memoirs 204, 261–278.
Álvarez, O., Gimenez, M., Braitenberg, C., Folguera, A., 2012. GOCE satellite derived gravity and gravity gradient corrected for topographic effect in the South Central Andes region. Geophys. J. Int. 190 (2), 941–959.
Álvarez, O., Nacif, S., Gimenez, M., Folguera, A., Braitenberg, C., 2014. GOCE derived vertical gravity gradient delineates great earthquake rupture zones along the Chilean margin. Tectonophysics 622, 198–215.
Álvarez, O., Gimenez, M., Folguera, A., Spagnotto, S., Bustos, E., Baez, W., Braitenberg, C., 2015. New evidence about the subduction of the Copiapó ridge beneath South America, and its connection with the Chilean-Pampean flat slab, tracked by satellite GOCE and EGM2008 models. Elsevier Editor. Syst. J. Geodyn. 91, 65–88.
Amante, C., Eakins, B.W., 2009. ETOPO1 1 Arc- Minute Global Relief Model: Procedures, Data Sources and Analysis, first ed. NOAA, National Geophysical Data Center, Boulder, Colorado, USA. pp: 54.
Anderson, M., Alvarado, P., Zandt, G., Beck, S., 2007. Geometry and brittle deformation of the subducting Nazca Plate, Central Chile and Argentina. Geophys. J. Int. 171 (1), 419–434.
Barazangi, M., Isacks, B., 1976. Spatial distribution of earthquakes and subduction of the Nazca plate beneath South America. Geology 4, 686–692.
Barazangi, M., Isacks, B.L., 1979. Subduction of the Nazca plate beneath Peru: evidence from spatial distribution of earthquakes. Geophys. J. Int. 57 (3), 537–555.
Barthelmes, F., 2009. Definition of Functionals of the Geopotential and their Calculation from Spherical Harmonic Models, 104132. http://publications.iass-potsdam.de/pubman/item/escidoc (3), 0902–2.
Barthelmes, F., 2014. Global Models. Encyclopedia of Geodesy. Springer International Publishing, pp. 1–9.
Blackwell, D.D., 1969. Heat-flow determinations in the northwestern United States. J. Geophys. Res. 74 (4), 992–1007.
Blackwell, D.D., 1971. The thermal structure of the continental crust. Struct. Phys. Prop. earth's crust 169–184.
Blakely, R., 1995. Potential Theory in Gravity and Magnetic Applications. Cambridge University Press, 441 pp.
Borzotta, E., Mamaní, M.J., Venencia, J.E., 2009. Preliminary Magnetotelluric study of Ambato and Valle Fértil Lineaments in Bermejo Basin and Sierra de Valle Fértil, San Juan, Argentina. Acta Geodaetica et Geophysica Hungarica 44 (2), 157–166.
Braitenberg, C., Mariani, P., Ebbing, J., Sprlak, M., 2011. The enigmatic Chad lineament revisited with global gravity and gravity-gradient fields. Geol. Soc. Lond. Spec. Publ. 357 (1), 329–341.
Briggs, I.C., 1974. Machine contouring using minimum curvature. Geophysics 39 (1), 39–48.
Brocher, T.M., 2005. Empirical relations between elastic wave speeds and density in the Earth's crust. Bull. Seismol. Soc. Am. 95 (6), 2081–2092.
Cahill, T., Isacks, B.L., 1992. Seismicity and shape of the subducted Nazca plate. J. Geophys. Res. Solid Earth 97 (B12), 17503–17529.
Cheesman, S., MacLeod, I., Hollyer, G., 1998. A new, rapid, automated grid stitching algorithm. Explor. Geophys. 29 (3/4), 301–305.
Chulick, G.S., Detweiler, S., Mooney, W.D., 2013. Seismic structure of the crust and uppermost mantle of South America and surrounding oceanic basins. J. S. Am. Earth Sci. 42, 260–276.
Cloos, M., 1993. Lithospheric buoyancy and collisional orogenesis: subduction of oceanic plateaus, continental margins, island arcs, spreading ridges, and seamounts. Geol. Soc. Am. Bull. 105 (6), 715–737.
Collo, G., Dávila, F.M., Nóbile, J., Astini, R.A., Gehrels, G., 2011. Clay mineralogy and thermal history of the Neogene Vinchina Basin, central Andes of Argentina: analysis of factors controlling the heating conditions. Tectonics 30 (4).
Collo, G., Ezpeleta, M., Dávila, F., Gimenez, M., Soler, S., Martina, F., Ávila, P., Sánchez-Nassif, F., Calegari, R., Lovecchio, J., Shiuma, M., 2017. Basin termal structure in the Chilean-Pampean flat subduction zone. In: The Making of the Chilean-argentinian Andes (in press).
Cornaglia, L., Ruiz, F., Introcaso, A., 2009. Análisis cortical de la cuenca Golfo de San Jorge utilizando anomalías de Bouguer y ondulaciones del geoide. Rev. la Asoc. Geol. Argent. 65 (3), 504–515.
Cortés, J., Casa, A., Yamin, M., Pasini, M., Terrizzano, C., 2014. Unidades morfotectónicas, estructuras oblicuas y patrones de distribución de la deformación cuaternaria en la precordillera de cuyo (28°-33°S). Actas XIX Congreso Geológico Argentino, Córdoba. S20-14.
Cortés, J.M., Casa, A., Pasini, M., Yamín, M., Terrizzano, C., 2006. Fajas oblicuas de deformación neotectónica en Precordillera y Cordillera Frontal (31° 30′ - 33° 30′ LS): controles paleotectónicos. Rev. la Asoc. Geol. Argent. 61 (4), 639–646.
Currie, C.A., Hyndman, R.D., Wang, K., Kostoglodov, V., 2002. Thermal models of the Mexico subduction zone: implications for the megathrust seismogenic zone. J. Geophys. Res. Solid Earth 107 (B12).
Dávila, F.M., Lithgow-Bertelloni, C., 2015. Dynamic uplift during slab flattening. Earth Planet. Sci. Lett. 425, 34–43.
Dobrin, M.B., 1976. Introduction to Geophysical Prospecting. McGraw-hill.
Förste, Christoph, Bruinsma, SeanL, Abrikosov, Oleg, Lemoine, Jean-Michel, Marty, Jean Charles, Flechtner, Frank, Balmino, G., Barthelmes, F., Biancale, R., 2014. EIGEN-6C4 the latest combined global gravity field model including GOCE data up to degree and order 2190 of GFZ Potsdam and GRGS Toulouse. GFZ Data Serv. https://doi.org/10.5880/icgem.2015.1.
Frost, B.R., Shive, P.N., 1986. Magnetic mineralogy of the lower continental crust. J. Geophys. Res. Solid Earth 91 (B6), 6513–6521.
Gans, C.R., Beck, S.L., Zandt, G., Gilbert, H., Alvarado, P., Anderson, M., Linkimer, L., 2011. Continental and oceanic crustal structure of the Pampean flat slab region, western Argentina, using receiver function analysis: new high-resolution results. Geophys. J. Int. 186 (1), 45–58. https://doi.org/10.1029/JB091iB06p06513. Journal of Geophysical Research. 91.6513–6521.
Garcia, E.S., Sandwell, D.T., Luttrell, K.M., 2015. An iterative spectral solution method for thin elastic plate flexure with variable rigidity. Geophys. J. Int. 200 (2), 1012–1028.
Gianni, G.M., García, H.P., Lupari, M., Pesce, A., Folguera, A., 2017. Plume overriding triggers shallow subduction and orogeny in the southern Central Andes. Gondwana Res. 49, 387–395.
Gilbert, H., Beck, S., Zandt, G., 2006. Lithospheric and upper mantle structure of central Chile and Argentina. Geophys. J. Int. 165 (1), 383–398.
Gimenez, M.E., Martinez, M.P., Jordan, T., Ruíz, F., Lince Klinger, F., 2009. Gravity characterization of the La Rioja valley basin, Argentina. Geophysics 74 (3), B83–B94.
Gutscher, M.A., Olivet, J.L., Aslanian, D., Eissen, J.P., Maury, R., 1999. The "lost Inca Plateau": cause of flat subduction beneath Peru? Earth Planet. Sci. Lett. 171 (3), 335–341.
Gutscher, M.A., Spakman, W., Bijwaard, H., Engdahl, E.R., 2000. Geodynamics of flat subduction: seismicity and tomographic constraints from the Andean margin. Tectonics 19 (5), 814–833.
Gutscher, M.A., 2002. Andean subduction styles and their effect on thermal structure and interplate coupling. J. S. Am. Earth Sci. 15 (1), 3–10.
Hamza, V.M., Cardoso, R.R., Ponte Neto, C.F., 2008. Spherical harmonic analysis of earth's conductive heat flow. Int. J. Earth Sci. 97 (2), 205–226.

Hamza, V.M., Gomes, A.J.L., Ferreira, L.E.T., 2005. Status report on geothermal energy developments in Brazil. Natural Gas 14, 7-5.
Henry, S.G., Pollack, H.N., 1988. Terrestrial heat flow above the Andean subduction zone in Bolivia and Peru. J. Geophys. Res. Solid Earth 93 (B12), 15153–15162.
Hinze, W.J., 2003. Bouguer reduction density, why 2.67? Geophysics 68 (5), 1559–1560.
Hinze, W.J., Von Frese, R.R., Saad, A.H., 2013. Gravity and Magnetic Exploration: Principles, Practices, and Applications. Cambridge University Press.
Hofmann-Wellenhof, B., Moritz, H., 2006. Physical Geodesy. Springer Science & Business Media.
Introcaso, A., 2006. Geodesia Física. Instituto de Fisiografía y Geología" Dr. Alfredo Castellanos".
Jones, R.E., De Hoog, J.C.M., Kirstein, L.A., Kasemann, S.A., Hinton, R., Elliott, T., Litvak, V.D., 2014. Temporal variations in the influence of the subducting slab on Central Andean arc magmas: evidence from boron isotope systematics. Earth Planet. Sci. Lett. 408, 390–401.
Jones, R.E., Kirstein, L.A., Kasemann, S.A., Dhuime, B., Elliott, T., Litvak, V.D., Alonso, R., Hinton, R., 2015. Geodynamic controls on the contamination of Cenozoic arc magmas in the southern Central Andes: insights from the O and Hf isotopic composition of zircon. Geochimica Cosmochimica Acta 164, 386–402.
Jones, R.E., Kirstein, L.A., Kasemann, S.A., Litvak, V.D., Poma, S., Alonso, R.N., Hinton, R., 2016. The role of changing geodynamics in the progressive contamination of Late Cretaceous to Late Miocene arc magmas in the southern Central Andes. Lithos 262, 169–191.
Jordan, T., Isacks, B., Allmendinger, R.W., Bewer, J., Ramos, V.A., Ando, C., 1983. Andean tectonics related to geometry of subducted Nazca Plate. Geol. Soc. Am. Bull. 94, 341–361.
Kane, M.F., 1962. A comprehensive system of terrain corrections using a digital computer. Geophysics 27 (4), 455–462.
Kay, S.M., Maksaev, V., Moscoso, R., Mpodozis, C., Nasi, C., Gordillo, C.E., 1988. Tertiary Andean magmatism in Chile and Argentina between 28 S and 33 S: Correlation of magmatic chemistry with a changing Benioff zone. J. S. Am. Earth Sci. 1 (1), 21–38.
Kay, S.M., Mpodozis, C., Ramos, V.A., Munizaga, F., 1991. Magma source variations for mid–late Tertiary magmatic rocks associated with a shallowing subduction zone and a thickening crust in the central Andes (28 to 33 S). Geol. Soc. Am. Special Pap. 265, 113–138.
Kay, S.M., Abbruzzi, J.M., 1996. Magmatic evidence for Neogene lithospheric evolution of the central Andean "flat-slab" between 30 S and 32 S. Tectonophysics 259 (1–3), 15–28.
Kay, S.M., Mpodozis, C., 2002. Magmatism as a probe to the Neogene shallowing of the Nazca plate beneath the modern Chilean flat-slab. J. S. Am. Earth Sci. 15 (1), 39–57.
Köther, N., Götze, H.J., Gutknecht, B.D., Jahr, T., Jentzsch, G., Lücke, O.H., Mahatsente, R., Sharma, R., Zeumann, S., 2012. The seismically active Andean and Central American margins: can satellite gravity map lithospheric structures? J. Geodyn. 59, 207–218.
Li, X., 2001. Vertical resolution: gravity versus vertical gravity gradient. Lead. Edge 20 (8), 901–904.
Li, C.F., Lu, Y., Wang, J., 2017. A global reference model of Curie-point depths based on EMAG2. Sci. Rep. 7.
Lince Klinger, F., Martinez, M.P., Gimenez, M.E., Ruiz, F., Álvarez, O., 2011. Modelo gravimétrico en la Fosa de Gastre, Provincia de Chubut, Argentina. Bol. Geol. Min. 122 (3), 299–310.
Lowry, A.R., Ribe, N.M., Smith, R.B., 2000. Dynamic elevation of the Cordillera, western United States. J. Geophys. Res. 105 (B10), 23–371.
Manea, V.C., Manea, M., Kostoglodov, V., Sewell, G., 2005. Thermo-mechanical model of the mantle wedge in Central Mexican subduction zone and a blob tracing approach for the magma transport. Phys. Earth Planet. Interiors 149 (1), 165–186.
Manea, V.C., Manea, M., 2011. Flat-slab thermal structure and evolution beneath central Mexico. Pure Appl. Geophys. 168 (8), 1475–1487.
Manea, V.C., Pérez-Gussinyé, M., Manea, M., 2012. Chilean flat slab subduction controlled by overriding plate thickness and trench rollback. Geology 40 (1), 35–38.
Manea, V.C., Manea, M., Ferrari, L., Orozco, T., Valenzuela, R.W., Husker, A., Kostoglodov, V., 2016. A review of the geodynamic evolution of flat slab subduction in Mexico, Peru, and Chile. Tectonophysics 695, 27–52.
Marot, M., Monfret, T., Gerbault, M., Nolet, G., Ranalli, G., Pardo, M., 2014. Flat versus normal subduction zones: a comparison based on 3-D regional traveltime tomography and petrological modelling of central Chile and western Argentina (29–35 S). Geophys. J. Int. 199 (3), 1633–1654.
Maus, S., Barckhausen, U., Berkenbosch, H., Bournas, N., Brozena, J., Childers, V., Dostaler, F., Fairhead, J.D., Finn, C., von Frese, R.R.B., Gaina, C., Golynsky, S., Kucks, R., Lühr, H., Milligan, P., Mogren, S., Müller, R.D., Olesen, O., Pilkington, M., Saltus, R., Schreckenberger, B., Thébault, E., Caratori Tontini, F., 2009. EMAG2: a 2–arc min resolution Earth Magnetic Anomaly Grid compiled from satellite, airborne, and marine magnetic measurements. Geochem. Geophys. Geosystems 10 (8).
Murphy, J.B., Oppliger, G.L., Brimhall, G.H., Hynes, A., 1998. Plume-modified orogeny: an example from the western United States. Geology 26, 731–734.
Nagy, D., 1966. The gravitational attraction of a right rectangular prism. Geophysics 31 (2), 362–371.
Oldenburg, D.W., 1974. The inversion and interpretation of gravity anomalies. Geophysics 39 (4), 526–536.
Parker, R.L., 1973. The rapid calculation of potential anomalies. Geophys. J. Int. 31 (4), 447–455.
Pavlis, N.K., Holmes, S.A., Kenyon, S.C., Factor, J.K., 2008. An earth gravitational model to degree 2160: EGM2008. EGU General Assem. 2008 (4), 4–2.
Pesce, A., Miranda, F. 2003. Catálogo de manifestaciones termales de la República Argentina. Vol. I-II Región Noroeste. SEGEMAR, Buenos Aires, 1666–3462.
Pilger, R.H., 1981. Plate reconstructions, aseismic ridges, and low-angle subduction beneath the Andes. Geol. Soc. Am. Bull. 92 (7), 448–456.
Ramos, V.A., Cristallini, E.C., Pérez, D.J., 2002. The pampean flat-slab of the central Andes. J. S. Am. Earth Sci. 15 (1), 59–78.
Ravat, D., Pignatelli, A., Nicolosi, I., Chiappini, M., 2007. A study of spectral methods of estimating the depth to the bottom of magnetic sources from near-surface magnetic anomaly data. Geophys. J. Int. 169 (2), 421–434.
Reguzzoni, M., Sampietro, D., 2015. GEMMA: an Earth crustal model based on GOCE satellite data. Int. J. Appl. Earth Obs. Geoinf. 35 (Part A), 31–43. https://doi.org/10.1016/j.jag.2014.04.002.
Ross, H.E., Blakely, R.J., Zoback, M.D., 2006. Testing the use of aeromagnetic data for the determination of Curie depth in California. Geophysics 71 (5), 51–59.
Roy, R.F., Blackwell, D.D., Decker, E.R., 1972. Continental heat flow. Nat. solid Earth 506–543.
Ruiz, F., Introcaso, A., 2004. Curie point depths beneath Precordillera Cuyana and Sierras Pampeanas obtained from spectral analysis of magnetic anomalies. Gondwana Res. 7 (4), 1133–1142.
Ruiz, F., Luna, E., Vargas, D., Gimenez, M., Martinez, P., 2011. Importancia del Ajuste y Nivelación de Datos Aeromagnéticos a partir de Magnetometría Terrestre. In: 18° Congreso Geológico Argentino, Actas, pp. 1198–1199 (Neuquén).
Sampietro, D., Reguzzoni, M., Negretti, M., 2013. The GEMMA crustal model: first validation and data distribution. In: Proceedings of the ESA Living Planet Symposium. ESA SP-722, Edinburgh (UK), 9–13 September 2013.
Sánchez, M.A., Winocur, D., Álvarez, O., Folguera, A., Martinez, M.P., 2017. Crustal structure of the high Andes in the North Pampean flat slab segment from magnetic and gravity data. J. S. Am. Earth Sci. 73, 153–167.
Shapiro, N.M., Ritzwoller, M.H., 2004. Thermodynamic constraints on seismic inversions. Geophys. J. Int. 157 (3), 1175–1188.
Smalley, R.F., Isacks, B.L., 1987. A high-resolution local network study of the Nazca Plate Wadati-Benioff Zone under western Argentina. J. Geophys. Res. Solid Earth 92 (B13), 13903–13912.
Soler, S.R., 2015. Métodos Espectrales para la Determinación de la Profundidad del Punto de Curie y Espesor Elástico de la Corteza Terrestre. Facultad de Ciencias Exactas, Ingeniería y Agrimensura (FCEIA), Universidad Nacional de Rosario (UNR) (Tesis de Grado para Título de Licenciado en Física. Inédito).
Springer, M., Förster, A., 1998. Heat-flow density across the Central Andean subduction zone. Tectonophysics 291 (1), 123–139.
Stauder, W., 1973. Mechanism and spatial distribution of Chilean earthquakes with relation to subduction of the oceanic plate. J. Geophys. Res. 78 (23), 5033–5061.
Tanaka, A., Okubo, Y., Matsubayashi, O., 1999. Curie point depth based on spectrum analysis of the magnetic anomaly data in East and Southeast Asia. Tectonophysics 306 (3), 461–470.
Tassara, A., Götze, H.J., Schmidt, S., Hackney, R., 2006. Three-dimensional density model of the Nazca plate and the Andean continental margin. J. Geophys. Res. Solid Earth 111 (B9).
Turcotte, D.L., Schubert, G., 2002. Geodynamics. Cambridge University Press, New York.
Vlaar, N.J., Van Keken, P.E., Van den Berg, A.P., 1994. Cooling of the Earth in the Archaean: consequences of pressure-release melting in a hotter mantle. Earth Planet. Sci. Lett. 121 (1–2), 1–18.
Van Hunen, J., Van Den BERG, A.P., Vlaar, N.J., 2002. On the role of subducting oceanic plateaus in the development of shallow flat subduction. Tectonophysics 352 (3), 317–333.
Watts, A.B., 2001. Isostasy and Flexure of the Lithosphere. Cambridge University Press.
Weidmann, C., Spagnotto, S., Giménez, M., Martínez, P., Álvarez, O., Sánchez, M., Lince Klinger, F., 2013. Crustal structure and tectonic setting of the south central Andes from gravimetric analysis. Geofís. Int. 197–208, 52-3.
Weidmann, C., Ariza, J.P., Sánchez, M., Gimenez, M., Christiansen, R., 2017. Magnetic crustal features in the Vinchina basin. J. S. Am. Earth Sci. 76, 94–100.
Ziagos, J.P., Blackwell, D.D., Mooser, F., 1985. Heat flow in southern Mexico and the thermal effects of subduction. J. Geophys. Res. Solid Earth 90 (B7), 5410–5420.

Please cite this article in press as: Sánchez, M.A., et al., Thermo-mechanical analysis of the Andean lithosphere over the Chilean-Pampean flat-slab region, Journal of South American Earth Sciences (2017), https://doi.org/10.1016/j.jsames.2017.09.036